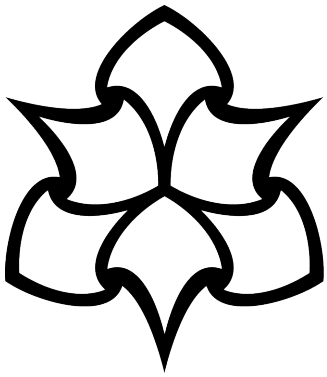

Examining the viability of the world's busiest winter road to climate change using a process-based lake model

*D.J. Mullan[1], I.D. Barr[2], R.P. Flood[1], J.M. Galloway[3], A.M.W. Newton[1], G.T. Swindles[1,4]

[1]Geography, School of Natural and Built Environment, Queen's University Belfast, Belfast, Northern Ireland, UK

[2]Department of Natural Science, Manchester Metropolitan University, Manchester, UK

[3]Geological Survey of Canada, Calgary, Alberta, Canada

[4]Ottawa-Carleton Geoscience Centre and Department of Earth Sciences, Carleton University, Ottawa, Ontario, Canada

*Corresponding Author Email: D.Mullan@qub.ac.uk

Abstract

Winter roads play a vital role in linking communities and building economies in the northern high latitudes. With these regions warming two to three times faster than the global average, climate change threatens the long-term viability of these important seasonal transport routes. We examine how climate change will impact the world's busiest heavy-haul winter road – the Tibbitt to Contwoyto Winter Road (TCWR) in northern Canada. The FLake freshwater lake model is used to project ice thickness for a lake at the start of the TCWR – first using observational climate data, and second using modelled future climate scenarios corresponding to varying rates of warming ranging from 1.5°C to 4°C above preindustrial temperatures. Our results suggest that 2°C warming could be a tipping point for the viability of the TCWR, requiring at best costly adaptation and at worst alternative forms of transportation. Containing

Early Online Release: This preliminary version has been accepted for publication in *Bulletin of the American Meteorological Society*, may be fully cited, and has been assigned DOI 10.1175/BAMS-D-20-0168.1. The final typeset copyedited article will replace the EOR at the above DOI when it is published.

warming to the more ambitious temperature target of 1.5°C pledged at the 2016 Paris Agreement may be the only way to keep the TCWR viable – albeit with a shortened annual operational season relative to present. More widely, we show that higher regional winter warming across much of the rest of Arctic North America threatens the long-term viability of winter roads at a continental scale. This underlines the importance of continued global efforts to curb greenhouse gas emissions to avoid many long-term and irreversible impacts of climate change.

Capsule

Warming of 2°C may be a tipping point for the world's busiest winter road, while enhanced winter warming threatens the viability of winter roads across Arctic North America.

Introduction

The Arctic has experienced warming two to three times greater than the long-term global mean trend of 0.87°C since preindustrial times (IPCC 2018), resulting in widespread shrinking of the cryosphere (IPCC 2019). This arctic amplification is projected to continue throughout the 21st century, with a 2°C global mean temperature increase (GMTI) projected to result in up to a 6°C warming in the Arctic (IPCC 2018). While impacts on ice sheets and glaciers tend to capture the headlines, there are also important consequences for infrastructure in Arctic and sub-Arctic communities, where warming temperatures threaten the physical integrity of overland transport routes and the economies they sustain (Meredith et al. 2019). Infrastructure built over permafrost is particularly vulnerable. Cumulative expenses of USD 5.5 billion are projected for climate-driven damage to public infrastructure in Alaska between 2015 and 2099 under high emissions scenarios, with one of the top two costs associated with building damage from near-surface permafrost thaw (Melvin et al. 2017). In a circumpolar study, Hjort et al.

Accepted for publication in *Bulletin of the American Meteorological Society.* DOI 10.1175/BAMS-D-20-0168.1.

(2018) revealed that nearly four million people and 70% of existing infrastructure in the permafrost domain lie in areas with high potential for near-surface permafrost thaw. Winter roads, comprising seasonally frozen sea, land, lakes, rivers, and creeks, are also under considerable threat from a warming climate. These seasonal roads are vital for the affordable transport of heavy equipment, cargo and fuel, but also provide physical connections that foster social and cultural interactions among remote communities (Chiotti and Lavender 2008; Furgal and Prowse 2008). In recent decades, climate change has shortened the operational season of winter roads across the Canadian Arctic, and published studies project future shortening in the James Bay region of Ontario (Hori et al. 2016; 2018); northern Manitoba and Saskatchewan (CIER 2006; Blair and Sauchyn 2010); the Mackenzie River, Northwest Territories (ACIA 2005); and the Tibbitt to Contwoyto Winter Road, Northwest Territories (Perrin et al. 2015; Mullan et al. 2017). One commonality in the methods used in these previous studies is that future projections are based on regression models developed between historic climate trends and ice thickness records. While there is merit in this statistical approach, it lacks a process-based incorporation of the multitude of meteorological and lake-specific parameters that influence the development of lake ice (Dibike et al. 2012). Given this limitation, the present study applies – for the first time – a process-based freshwater lake model to simulate the impacts of climate change on winter roads. We do this by examining the future viability of the world's busiest heavy-haul winter road to GMTIs of 1.5°C, 2°C and 4°C above preindustrial temperatures. We also make inferences for the future viability of other winter roads across Arctic North America based on projected winter warming in the region.

Study Region, Materials and Methods

The study region is the Tibbitt to Contwoyto Winter Road (TCWR), Canada – a seasonally operational winter road extending from Tibbitt Lake, Northwest Territories ~ 70 km east of

Accepted for publication in *Bulletin of the American Meteorological Society.* DOI 10.1175/BAMS-D-20-0168.1.

Yellowknife and spanning around 400 km northwards across frozen lakes (85%) and overland portages (15%) to Ekati diamond mine, north of Lac de Gras (JVTC 2020) (Figure 1). The TCWR is of considerable economic importance as the only overland transport route supplying four mines with fuel, cement, tyres, explosives, and other construction and maintenance materials to a value of CAD 500 million yr^{-1} (JVMC 2015). It is the busiest heavy-haul winter road in the world, with more than 300,000 tonnes transported in over 10,000 loads yr^{-1} (Perrin et al. 2015). This annual haulage has, on average, been squeezed into a shorter transport season (herein referred to as the operational season) over the past twenty years, at least in part driven by rising air temperatures in the region (Appendix Figure A1).

A modelling approach

We simulate ice thickness for Tibbitt Lake (62.56°N, 113.36°W) at the southern limit of the TCWR using the FLake freshwater lake model (http://www.flake.igb-berlin.de/site/download) (Kirillin et al. 2011). FLake simulates the vertical temperature structure and mixing conditions of shallow lakes (≤ 50 m) (Huang et al, 2019). It is used as a lake parameterisation module in three-dimensional numerical weather prediction and climate models, but can also run in stand-alone mode as a single-column lake model (Mironov 2008). We apply FLake in stand-alone mode, simulating ice thickness for 20-year simulations at a daily time step representing (1) observed climate, and (2) a set of 15 future climate scenarios. We applied the model on a hydrological year basis – with each year beginning on 1 October and ending on 30 September. This approach is employed to ensure model simulations begin prior to the annual onset of ice freeze up.

Simulations under observed climate

Accepted for publication in *Bulletin of the American Meteorological Society.* DOI 10.1175/BAMS-D-20-0168.1.

FLake first requires a set of lake-specific parameters. Lake depth (6.7 m) was taken from Crann et al. (2015) and fetch (2000 m) was approximated by maximum lake length, measured using Google Earth™. The extinction coefficient (0.6 m^{-1}) for water transparency was estimated from field notes associated with Galloway et al. (2010) – a number representing clear water. For a 0.5° x 0.5° grid square containing Tibbitt Lake, daily mean temperatures, relative humidity, solar radiation, and wind speed data from 1 October 1985 – 30 September 2005 were taken from the Watch Forcing Dataset Era Interim (WFDEI) (Weedon et al. 2014), accessed through the Earth System Grid Federation (ESGF) (https://esgf-node.llnl.gov/). Cloud cover data were unavailable from WFDEI and instead taken from the European Centre for Medium-Range Weather Forecasts (ECMWF) next-generation reanalysis (ERA5) (C3S 2017), accessed through the Copernicus Climate Data Store (CDS) (https://cds.climate.copernicus.eu/) for a 0.5° x 0.5° grid square containing Tibbitt Lake. The October 1985 – September 2005 time period was chosen for two reasons: (1) the observational data are required to bias correct future climate scenarios in a later step based on its comparison to a model hindcast period, with most model hindcast periods ending in 2005; and (2) 1986-2005 is the historical baseline period used by the Intergovernmental Panel on Climate Change (IPCC) in their Fifth Assessment Report (AR5) (IPCC 2013). FLake was run under the observed climate, with dates recorded when lake ice thickness exceeded 107 cm (the safe minimum limit for heavy-haul vehicles) (Perrin et al. 2015). Since there are no measured ice thickness data for Tibbitt Lake, we compared measured records for four analagous shallow sub-arctic Canadian lakes (locations shown in Figure 1) with FLake simulations for the same lakes. The measured data were taken from Environment and Climate Change Canada (Environment and Climate Change Canada, 2020) and were available for a minimum of 10 years between 1981 and 2000, with FLake simulations run for the same years following an identical approach to input data as described above for Tibbitt Lake. Validation results indicate the model has a tendency to underestimate ice thickness early

Accepted for publication in *Bulletin of the American Meteorological Society.* DOI 10.1175/BAMS-D-20-0168.1.

and late in the lake ice season, while observed ice thickness in the heart of the lake ice season is generally overestimated (Appendix Text A1, Figure A2).

Simulations under future climate

FLake was then run under a series of future climate scenarios corresponding to GMTIs of 1.5°C, 2°C and 4°C. The former two rates of warming reflect pledges made by 195 countries under the 2016 Paris Agreement (UNFCCC 2015) and are therefore considered mitigation scenarios, whereas the latter represents something approximating a no-mitigation scenario – a rate of warming evaluated as being *as likely as not* to be exceeded by the end of the 21st century under the highest representative concentration pathway (RCP) 8.5 (IPCC 2013). To account for arctic amplification we examined how the selected GMTIs corresponded to warming in the study region and found that 1.5°C, 2°C and 4°C equated to 2.9°C, 3.9°C and 7.8°C (Appendix Text A2). These are herein referred to as regional mean temperature increases (RMTIs). For each RMTI, we shortlisted five climate scenarios (n=15) from an initial pool of 82 available, based on how closely they compared to observations at a monthly temporal resolution for a hindcast period from 1986-2005 (Appendix Text A3, Table A1). Daily mean temperatures from the 15 model scenarios were then downloaded from the ESGF and CDS for the grid square containing Tibbitt Lake. All scenarios are part of the Coupled Model Intercomparison Project (CMIP5) (Taylor et al. 2012), forced with RCP8.5 (van Vuuren et al. 2011) – a high radiative forcing scenario necessary to capture RMTIs up to 7.8°C. For each scenario, we extracted the 20-year future time period when projected temperatures reached 2.9°C, 3.9°C and 7.8°C above preindustrial temperatures. Projected temperatures were bias corrected using the change factor methodology used in Ho et al. (2012) (Appendix Text A4). Only temperatures were modified from the baseline FLake simulations, with the other meteorological parameters left constant. This reflects the dominant role that air temperatures play in changing lake ice conditions

Accepted for publication in *Bulletin of the American Meteorological Society.* DOI 10.1175/BAMS-D-20-0168.1.

(Brown and Duguay 2010), but also the fact that some of the other meteorological parameters are unavailable from many of the selected climate models. FLake was then run under each projected climate scenario and the dates recorded when lake ice thickness exceeded the 107 cm threshold. The projected operational season of the TCWR for each model was adjusted to reflect the difference between the baseline simulations and the historical operational season of the TCWR (JVTC 2020) (Appendix Text A5). We also downloaded temperatures for the period 1 October 2000 – 31 September 2020 from ERA5 (C3S 2017) to capture years post-2005 and allow us to relate these to the TCWR operational season observations. Present and future operational season length was then colour coded in a traffic light system based on an economic analysis conducted by Perrin et al. (2015). Green indicates ≥ 50 days – a viable season; amber indicates 45-49 days – an 'adaptive scenario' where flexible scheduling is required to meet season demands at a high cost of around USD 1.57 million yr^{-1}; and red indicates < 45 days – a 'critical conditions scenario' representative of an unviable season and the need for alternative transportation at a cost of around USD 6.09 million yr^{-1}.

Providing wider geographical context

In order to set our results for the TCWR within a wider geographical context, we downloaded monthly observed temperatures from ERA5 (C3S 2017) and monthly CMIP5 climate model scenarios for each of the 15 future scenarios used in the FLake simulations for the northern half of North America (40°N – 90°N, 55° – 180°W). Future scenarios were interpolated to the same resolution as the observed data and then bias corrected using a change factor approach, by subtracting the hindcast period of the model from the future period and adding the result to observations (Hawkins et al. 2013).

Results and Discussion

Accepted for publication in *Bulletin of the American Meteorological Society.* DOI 10.1175/BAMS-D-20-0168.1.

Projected changes in the TCWR operational season relative to the present are shown in Figure 2. The mean length of the operational season is projected to decrease for all but one of the 15 future scenarios, from 61 days at present to 56-61 days under 1.5°C, 47-55 days under 2°C and 20-31 days under 4°C. The range reflects differences in climate model scenarios. Although not directly comparable because we focus on rates of warming rather than set time periods, changes are broadly in line with previous projections for the TCWR. Perrin et al. (2015) projected a mean operational season of 58 days by the 2020s and 49 days by the 2050s, while a much shorter operational season of 21, 5 and 2 days was projected by Mullan et al. (2017) for the 2020s, 2050s and 2080s respectively. The particularly extreme scenarios in the latter may reflect limitations in the regression modelling methodology, lending support to the process-based lake modelling conducted here. According to the Perrin et al. (2015) classification, our results suggest that warming of 1.5°C permits a viable TCWR operational season, but an increase to 2°C leads to costly adaptation under two scenarios. A warming of 4°C shows a mean operational season well below the unviable threshold, indicating no future for the TCWR before this level of warming is reached. These findings suggest that, for an average year, an increase from 1.5°C to 2°C is the tipping point at which costly adaptation is required. An increase from 1.5°C to 2°C GMTI was also found to impose higher risks for a number of other natural and human systems, including in some cases long-lasting or irreversible impacts such as the loss of some ecosystems (IPCC 2018).

Enhanced December warming and impacts on late opening

From the present mean operational season of 31 January to 1 April, future changes in the mean operational season length translates to 30 January-3 February to 29-31 March under 1.5°C, 4-10 February to 26-30 March under 2°C and 18-27 February to 17-20 March under 4°C (Figure 2). These dates reveal there is a general trend towards a larger proportion of the change coming

Accepted for publication in *Bulletin of the American Meteorological Society.* DOI 10.1175/BAMS-D-20-0168.1.

from a delayed opening – particularly at 4°C – with a slower rate of change in an earlier closure. Jensen et al. (2007) found a similar pattern across 65 water bodies in the Great Lakes region between Minnesota and New York, USA – with lake freeze up occurring 3.3 days decade^{-1} later and lake breakup occurring at a slower rate of 2.1 days decade^{-1} earlier from 1975-2004. Figure 3 explains the trend towards a greater proportion of change from a delayed opening in this study, with November-January temperatures projected to warm at a rate far in excess of February-April temperatures. For example, under a GMTI of 4°C, December temperatures in the Tibbit Lake region are projected to warm by 11.5°C compared to a 6.1°C rise in March. Temperatures in the autumn months generally act as the dominant control on lake and river ice freeze up, with reduced autumn cooling known to prolong the period of above zero water temperatures and delay the onset of freeze up (Prowse et al. 2007). Hori et al. (2018) refer to these months, primarily October-December in the high latitudes, as the preconditioning period of winter roads – essential for providing a more climatically favourable construction period and contributing to earlier opening dates. When warming of the magnitude projected here occurs during this preconditioning period, it is unsurprising that a considerable delay in the opening of the TCWR follows. Figure 3 reveals this pattern could be expected to an even larger degree across much of the rest of Arctic North America, with a GMTI of 1.5°C, 2°C and 4°C resulting in regional December warming in excess of 5°C, 8°C and 15°C across parts of the Prudhoe Bay coast of Alaska, the Northwest Territories, Nunavut, and the Hudson Bay coastal regions of Manitoba, Ontario and Quebec. With a number of prominent winter roads in these regions, a widespread shift towards costly adaptation or route closure seems likely.

The levels of winter warming projected here – in places over three times the global average – are consistent with projections for the Arctic by the end of the 21st century (IPCC 2013; 2019). These high rates of warming can be explained by a projected continuation of arctic

Accepted for publication in *Bulletin of the American Meteorological Society.* DOI 10.1175/BAMS-D-20-0168.1.

amplification, where observed records in recent decades show a warming signal that has been strongest over the Arctic Ocean in autumn and winter (Cohen et al. 2014; Horton et al. 2015). A number of mechanisms are thought to be responsible for enhanced sensitivity to warming in the Arctic, but chief among them is the change in sea ice albedo owing to the stark difference in reflective properties of an ice-free ocean and snow-covered sea ice surfaces (*ca.* 7% vs 80% reflectance respectively) (Cohen et al. 2019). This likely explains the high degree of warming particularly along the Arctic coastal regions in autumn and winter (Figure 3). Other more localised arctic amplification mechanisms may contribute to enhanced autumn and winter warming in the study region, located ~ 500 km south of the Arctic coast. Local forcings include snow, cloud and ice insulation feedbacks (Kwok et al. 2009; Lee et al. 2011; Yang and Magnusdottir 2018), while increased vegetation over Arctic land contributes to surface darkening at high latitudes (Overland et al. 2015). It is thought that local and remote forcing mechanisms may interact and amplify one another (Yang and Magnusdottir 2018), meaning some combination of all the above factors is likely at play in amplifying warming in the wider TCWR region. Attribution studies indicate that increasing anthropogenic greenhouse gases play a vital role in driving Arctic surface temperature increases (Fyfe et al. 2013; Najafi et al. 2015), leading to a high confidence in projections of further Arctic warming (Overland et al. 2018).

Interannual variability

The interannual variability within the 20-year observations and simulation periods reveals that mean patterns are subject to considerable divergence from year to year, as shown in Figure 4. During the observed period, the TCWR opened as late as 9 February in 2016 (9 days later than the mean), while it closed as early as 21 March in 2010 (11 days earlier than the mean). As seen in Figure 4 and in Figure A1, shortened seasons are often associated with anomalously

Accepted for publication in *Bulletin of the American Meteorological Society.* DOI 10.1175/BAMS-D-20-0168.1.

warm years, partly due to large-scale teleconnections that correlate most strongly with Canadian climate during winter (Bonsal and Shabbar 2011). Anomalous heating in the Eastern tropical Pacific associated with El Niño results in a positive Pacific-North American (PNA) pattern over North America (Wallace and Gutzler 1981) and consequently warmer than average temperatures from late autumn to early spring (Shabbar and Khandekar 1996). The two shortest operational seasons on record (2010: 46 days; and 2016: 44 days) follow two of the strongest El Niño events in recent decades: 2009/10 and 2015/16 (Timmermann et al. 2018). Shorter operational seasons in some cases may also be associated with increased winter storminess. Major storms with high wind speeds and blowing snow can cause temporary closures on the road, as occurred in March 2012 (Rodan 2012). Where anomalously warm or stormy winters cause the ice to break open in a 'blowout' (Ashbury 2006), winter roads may shut for maintenance or may even close for the season. The short 50-day season in 2006 occurred in such a way, with a blowout on Waite Lake late in the season (14 March) before the season was complete (Perrin et al. 2015). Consequently, approximately 1,200 loads were flown into mines in the summer and autumn of 2006 at a cost of CAD 100-150 million (JVMC 2014; Perrin et al. 2015). A poleward shift in extratropical cyclone activity is projected to result in increased atmospheric moisture and greater winter precipitation over the northern half of North America (Christensen et al. 2013). This indicates the clear future potential for an increase in blowing snow and hazardous blizzards that further threaten the operational season of the TCWR. Conversely, longer operational seasons are typically associated with colder than average years. For example, the longest operational season on record (26 January – 16 April 2002: 81 days) occurred when 2001/02 winter and early 2002 spring temperatures were considerably colder than average. Cooler years are typically associated with modes of variability in opposite phases to anomalously warm years. A switch towards La Niña events and a negative phase of the PNA are associated with earlier freeze up and later breakup of lake and river ice across much of

Accepted for publication in *Bulletin of the American Meteorological Society.* DOI 10.1175/BAMS-D-20-0168.1.

Canada (Bonsal et al. 2006). Figure 4 shows that interannual variability in temperatures and the winter road operational season are projected to continue in future, indicating that natural variability will continue to result in considerable year to year divergence from the mean. Figure 2 shows that the year with the longest projected operational season under 1.5°C (69-79 days) and 2°C (63-72 days) is always longer than the mean observed season (61 days) and reflective of a viable season in the Perrin et al. (2015) classification. In addition, Figure 2 shows that the mean projected operational season is always longer at 1.5°C (56-61 days) and 2°C (47-55 days) than it is during the shortest year of the observed record (44 days). Figure 5 reveals the reason for this, as temperature anomalies during the warmest observed year are higher than the mean temperature anomalies for 1.5°C and 2°C for all months under most future scenarios (note this refers to the warmest observed year out of 20 simulated years, where the actual year may differ between months). Furthermore, the year with the longest projected operational season at 4°C (37-50 days) is for two models greater than the shortest observed operational season (44 days). Figure 5 again shows why, since the year with coldest projected temperatures under 4°C is colder than the warmest observed year during January-April. In this sense, greater future variability may offer hope that colder than average years could permit some fully operational seasons, even when the mean suggests otherwise. For example, under the least extreme 2°C model – where a mean operational season of 55 days is projected – there are 12 years out of 20 where a fully viable season up to the longest year of 72 days is projected.

However, greater future variability also means there are several years that fall below the mean. The same 2°C scenario referred to above has a shortest season length of 36 days and eight out of 20 years that fall below the 50-day threshold. Considering the shortened 50-day season and associated high costs in 2006, it is clear that scenarios such as the one identified above do not lend support to a viable TCWR without at least considerable adaptation. Even under 1.5°C

Accepted for publication in *Bulletin of the American Meteorological Society.* DOI 10.1175/BAMS-D-20-0168.1.

scenarios, where the mean operational seasons of all five models exceed the 50-day threshold, shortest seasons lie below 40 days – with several years among the 20-year projections falling below the viable threshold. For example, under the least extreme 1.5°C model – where the mean season length is 61 days – there are still four years out of 20 where the operational season is less than 50 days. Falling short of a viable season length at a frequency of once every five years may raise important questions among planners about the long-term viability of the TCWR. That outlook becomes even bleaker when we examine the most extreme 1.5°C and 2°C scenarios, with seven out of 20 years below the 50-day threshold for the former, and 11 years for the latter. At 4°C, the TCWR is unequivocally unviable. Three out of five models under the 4°C scenarios project all 20 years to fall below the 50-day threshold, with the other two models projecting only one or two years respectively above this threshold. As shown in Figure 5, temperatures rising above freezing in November and April under these scenarios indicates why such large reductions in the operational season are simulated.

Adaptation

Before considering costly large-scale adaptation options, there are first adaptations to present-day practices that may help ensure the TCWR remains viable for longer. Sladen et al. (2020) investigated threshold requirements for the initiation of winter road operations along the TCWR and found that the current practice of planning construction by calendar dates rather than by evaluation of air-freezing indices results in a conservative approach to the start of the construction season. In the interests of 'winning back' some time as the climate reduces the length of the operational season, it may be necessary to adapt a more methods-based approach to the dates of winter road construction, by installing equipment to calculate freezing indices or measure frozen ground depths and temperatures. It is also clear, however, that such an approach incurs expense, logistical challenges and issues with mobilising equipment and

Accepted for publication in *Bulletin of the American Meteorological Society.* DOI 10.1175/BAMS-D-20-0168.1.

personnel at short notice (Sladen et al. 2020). Amending the nature of annual haulage on the TCWR may also represent a low-cost adaptation measure in the face of shortening operational seasons. For winter roads linking remote communities, the desire is to ensure as long a season as possible. This is not the case for the TCWR, where the goal is to ensure specified tonnages of materials to mines are provided during the operational season. Where the season length is reduced, lost service may be recovered by increasing the number of daily loads (Perrin et al. 2015). We see evidence of this in the historical records (Appendix Table A2) – years with a reduced operational season but higher freight statistics than years with a longer season. For example, 2016 ranks third out of 20 years for highest number of loads (8,766) and tonnes transported (262,261), despite being the shortest operational year (44 days) on record. This clearly shows there is some scheduling flexibility that can help offset a shortened operational season. The limiting factor in this scenario is the number of trucks and drivers available (Perrin et al. 2015). Increasing their provision to facilitate maximising the daily use of the TCWR may therefore avoid more costly adaptation. The above adaptations may help under the less extreme scenarios highlighted in this study, but larger-scale higher-cost alternatives may be needed under more extreme scenarios. Options already considered for the TCWR include construction of an all-season gravel-surface overland route along the most vulnerable southern portion; construction of a deep sea port at Bathurst Inlet, Nunavut, with a road to the mines across colder Arctic tundra; and construction of 600 km of power lines to expand hydroelectric power and reduce reliance of the mines on diesel – the most transported commodity in the TCWR (Perrin et al. 2015). If pledges to reduce greenhouse gas emissions are not met, there may be little alternative but to implement one or more of these measures to protect economic activity in the region.

Conclusions, Limitations and Future Work

Accepted for publication in *Bulletin of the American Meteorological Society.* DOI 10.1175/BAMS-D-20-0168.1.

Unlike previous studies, use of a process-based freshwater lake model has allowed us to incorporate more of the factors influencing the development and evolution of lake ice along the TCWR. Despite this, there are a number of limitations that must be considered when interpreting the results. FLake has been found to overestimate ice thickness (e.g. Kheyrollah Pour et al., 2012) – a trend clearly evident in our validation (Figure A2) during the peak cold season between January and March. We also identified an underestimation of ice thickness in November/December and in April/May, corresponding with slightly later than observed freezeup (by 3 days on average) and earlier breakup (by 9 days on average). These freezeup/breakup trends are similar to some studies (e.g. Kheyrollah Pour et al., 2012; Rontu et al., 2019) and opposite in sign to others (e.g. Yang et al., 2013; Kourzeneva, 2014; Peitikäinen et al., 2018). Timing of overestimation and underestimation in our validation results likely points to difficulties in simulating the accumulation of snow on lake ice (Rontu et al., 2019). FLake does not account for the insulating effect of snow, meaning ice is able to thicken more rapidly but also melt faster without snow buffering ice from the cold air above (Jeffries and Morris, 2006). Although provision is made to model parametrically the evolution of snow cover above lake ice in FLake, the model has not been sufficiently tested in this regard and is highlighted as an area requiring development (FLake, 2020). It is not possible to quantify in days the potential impact this limitation has on the operational season length of the TCWR, but we highlight this as a particular point of caution when interpreting the projected dates shown in Figure 2. The daily time step may be too temporally coarse to take account of important processes relating to ice formation, including low wind speeds and calm events creating the potential for complete lake freeze within hours (Bernhardt et al., 2011). This highlights another important issue – only air temperatures were modified in the future simulations owing to data availability. This limits the reliability of future projections since interactions with other changing meteorological properties including wind speed are essential components in ensuring

Accepted for publication in *Bulletin of the American Meteorological Society.* DOI 10.1175/BAMS-D-20-0168.1.

vertical heat transfer is sufficient to cool surface water temperatures to 0°C (Leppäranta, 2010; Nõges and Nõges, 2014). Perturbing other meteorological variables in the model in addition to mean temperatures would build a fuller picture of the impacts of climate change on the TCWR. No ice thickness measurements were available for Tibbitt Lake, so it is not possible to fully evaluate model performance for the lake simulated in this study. Future studies could also build on our progress by accounting for the ~ 15% of the TCWR route crossing overland portages, which primarily comprise permafrost peatlands (Sladen et al. 2020). With rapid thawing of permafrost peatlands in the Canadian Arctic (Swindles et al. 2015; Sim et al. 2019), it is currently unclear if these sections of the TCWR are more or less vulnerable to warming than lakes. Finally, a continental or hemispheric-scale study simulating the impacts of climate change on other winter roads across the high latitudes, beyond the inferences we have made, would be highly valuable. In the meantime, our work represents a considerable advance on previous studies and highlights the escalating threat that climate change poses to the future viability of the TCWR and most likely other North American winter roads. The identification of a tipping point at 2°C GMTI illustrates that the actions of current and future generations in cutting greenhouse gas emissions is critical to the future viability of winter roads and the vital role they provide in building economies and linking communities in the northern high latitudes.

Acknowledgments

The authors acknowledge helpful feedback received on the manuscript from Steve Grasby, Geological Survey of Canada.

Data Availability Statement

Accepted for publication in *Bulletin of the American Meteorological Society.* DOI 10.1175/BAMS-D-20-0168.1.

References to the datasets used in this study and the web addresses for the data repositories they were downloaded from can be found in the Datasets, Materials and Methods sections (and in Appendix Text A1 and A2). All data are freely and openly available.

Appendix Text

Text A1. FLake Model Validation

Ice thickness data for four lakes in Canada were downloaded from Environment and Climate Change Canada. We selected the four lakes following a careful screening process that started by examining all available lake ice records from Environment and Climate Change Canada and including those lakes that fulfilled the following criteria: (1) latitude > 52.5° (to ensure lakes are within 10° of the study lake); (2) > 10 years of data between 1981-2000 (to correspond with the modelling time period for the study lake); and (3) lakes with a mean depth < 50 m (as determined from the Global Lake Database) – note 50 m depth is considered the upper limit of suitability for FLake modelling. This generated a validation database comprising four lakes – the details of which are provided in Figure A2. Measurements for these four lakes exist at approximately a weekly temporal resolution and were measured to the nearest centimetre using a special auger kit or hot wire ice thickness gauge (Environment Canada, 2020). FLake simulations were run from 1 October 1981 – 30 September 2000 and were then compared to the observed ice thickness records by extracting modelled ice thickness only for the precise dates where measured data existed during the 19-year comparison period. The two sets of data were then compared for the (inclusive) months November-May, with the absolute error, mean absolute error and percentage error calculated to determine the degree to which the model under or overestimated ice thickness during these months (Figure A2). We also downloaded observed freezeup and breakup dates for each validation lake from the Global Lake and River Ice

Accepted for publication in *Bulletin of the American Meteorological Society.* DOI 10.1175/BAMS-D-20-0168.1.

Phenology Database Version 1 (Benson et al., 2020) and compared these records with FLake simulated freezeup and breakup dates for the same years as the data used to calculate absolute error (Figure A2).

Text A2. Calculating RMTIs

To calculate RMTIs for the study area, monthly mean temperatures were downloaded from KNMI Climate Explorer (https://climexp.knmi.nl/). Historical monthly mean temperatures for the period 1986-2005 were subtracted from the 2006-2100 period forced with RCP8.5 for the mean of all CMIP5 models and ensembles. This was done for the global average (resulting in 2.0°C) and subsequently for the grid square containing Tibbitt Lake (resulting in 3.9°C). This global : regional ratio of 2.0 : 3.9 was subsequently used to correct GMTIs of 1.5°C, 2°C and 4°C by simply dividing 3.9 by 2.0 and multiplying by the relevant GMTI. This produced RMTIs of 2.9°C 3.9°C and 7.8°C. We deducted 0.6 from each RMTI to reflect the fact that the 1986-2005 period was 0.6°C warmer than preindustrial temperatures, and then calculated the mean 20-year period when temperatures were 2.3°C, 3.3°C and 7.2°C higher than the 1986-2005 hindcast period for each model.

Text A3. Shortlisting climate models

We downloaded all available CMIP5 models and ensembles at a monthly temporal resolution under RCP8.5 (n=82) for the grid square containing Tibbitt Lake. For all 82 scenarios, we calculated the root mean squared error (RMSE) from the difference between the 1986-2005 historical temperatures for that scenario and the 1986-2005 observed temperatures for Tibbitt Lake. The 82 scenarios were ranked by their RMSE and the top five for each GMTI shortlisted for subsequent FLake modelling. In several cases, a different 20 year future time period from

Accepted for publication in *Bulletin of the American Meteorological Society.* DOI 10.1175/BAMS-D-20-0168.1.

the same scenario was used among the final 15 scenarios. The full list of selected scenarios and extracted time periods is given in Table A1.

Text A4. Bias Correction

Daily temperature projections for each scenario were bias corrected using a change factor (CF) methodology that uses observed daily variability and changes the mean and daily variance as simulated by the model (e.g. Arnell et al. 2003, Gosling et al. 2009). Outlined in Ho et al (2012), this method takes the form:

$$T_{CF}(t) = \overline{T_{RAW}} + \frac{\sigma T_{RAW}}{\sigma T_{REF}} \left(O_{REF}(t) - \overline{T_{REF}}\right)$$

Where T_{RAW} represents daily raw model output for the future period, T_{REF} represents daily raw model output for the historical period, O_{REF} represents daily observed output, time (t) represents a daily time step, the bar above a symbol denotes the mean, and σ represents standard deviation.

Text A5. Operational Season Adjustment

Projected operational season dates were adjusted using the following equation:

$$D_{AdjOBS} = \left(\frac{D_{REF}}{D_{OBS}}\right)\left(D_{FUT} - D_{OBS}\right)$$

Where D_{AdjOBS} represents adjusted projected operational season dates, D_{REF} represents projected operational dates for the baseline simulations, D_{OBS} represents operational dates from historical records (2001-2020), and D_{FUT} represents projected operational dates from future simulations.

Accepted for publication in *Bulletin of the American Meteorological Society.* DOI 10.1175/BAMS-D-20-0168.1.

References

ACIA, 2005: Arctic climate impact assessment. Cambridge University Press, Cambridge.

Arnell, N. W., D. A. Hudson, and R. G. Jones, 2003: Climate change scenarios from a regional climate model: estimating change in runoff in southern Africa. *J. Geophys. Res.*, **108**, 4519-4535, https://doi.org/10.1029/2002JD002782.

Ashbury, D., 2006: Over the top. Rio Tinto Review, No. 79: 9–14.

Benson, B., J. Magnuson, and S. Sharma, 2020: Global Lake and River Ice Phenology Database, Version 1. Boulder, Colorado USA. NSIDC: National Snow and Ice Data Center. Accessed 20 March 2021, https://doi.org/10.7265/N5W66HP8.

Bernhardt, J., C. Engelhardt, G. Kirillin, and J. Matschullat, 2012: Lake ice phenology in Berlin-Brandenburg from 1947-2007: observations and model hindcasts. *Clim. Change*, **112**, 791-817, DOI 10.1007/s10584-011-0248-9.

Blair, D., and D. Sauchyn, 2010: Winter roads in Manitoba, In: Sauchyn, D., H. Diaz, S. Kulshreshtha (Eds.) The new normal: the Canadian prairies in a changing climate. CPRC Press, Regina, pp. 322-325.

Bonsal, B. R., T. D. Prowse, C. R. Duguay, and M. P. Lacroix, 2006: Impacts of large-scale teleconnections on freshwater-ice break/freeze-up dates over Canada. *J. Hydrol.*, **330**, 340-353, https://doi.org/10.1016/j.jhydrol.2006.03.022.

Bonsal, B., and A. Shabbar, 2011: Large-scale climate oscillations influencing Canada, 1900-2008. Canadian Biodiversity: Ecosystem Status and Trends 2010. Technical Thematic Report No. 4. Canadian Councils of Resource Ministers, Ottawa, ON. Accessed 19 May 2020, https://biodivcanada.chm-cbd.net/sites/biodivcanada/files/2018-02/974No.4_Climate%20Oscillations%20April%202011_E.pdf.

Accepted for publication in *Bulletin of the American Meteorological Society*. DOI 10.1175/BAMS-D-20-0168.1.

494 Brown, L. C., and C. R. Duguay, 2010: The response and role of ice cover in lake-climate
495 interactions. *Prog. Phys. Geog.*, **34 (5)**, 671-704,
496 https://doi.org/10.1177/0309133310375653.

497 Chiotti, Q., and B. Lavender, 2008: Ontario, In: Lemmen, D. S., F. J. Warren, J. Lacroix, E.
498 Bush (Eds.) From impacts to adaptation: Canada in a changing climate 2007. Government
499 of Canada, Ottawa, pp. 227-274.

500 Christensen, J. H., and Coauthors, 2013: Climate Phenomena and their Relevance for Future
501 Regional Climate Change. In: Climate Change 2013: The Physical Science Basis.
502 Contribution of Working Group I to the Fifth Assessment Report of the Intergovernmental
503 Panel on Climate Change [Stocker, T.F., and Coauthors (eds.)]. Cambridge University
504 Press, Cambridge, United Kingdom and New York, NY, USA.

505 CIER, 2006: Climate change impacts on ice, winter roads, access trails, and Manitoba First
506 Nations. Accessed 16 June 2012,
507 http://www.nrcan.gc.ca/earthsciences/projdb/pdf/187b_e.pdf.

508 Cohen, J., and Coauthors, 2019: Divergent consensuses on arctic amplification influence on
509 midlatitude severe winter weather. *Nature*, **10**, 20-29, https://doi.org/10.1038/s41558-019-
510 0662-y.

511 Cohen, J., and Coauthors, 2014: Recent arctic amplification and extreme mid-latitude weather.
512 *Nat. Geosci.*, **7**, 627-637, https://doi.org/10.1038/ngeo2234.

513 Copernicus Climate Change Service (C3S), 2017: ERA5: Fifth generation of ECMWF
514 atmospheric reanalyses of the global climate. Copernicus Climate Change Service Climate
515 Data Store (CDS), Accessed 19 May 2020,
516 https://cds.climate.copernicus.eu/cdsapp#!/home.

Accepted for publication in *Bulletin of the American Meteorological Society*. DOI 10.1175/BAMS-D-20-0168.1.

517 Crann, C. A., R. T. Patterson, A. L. Macumber, J. M. Galloway, H. M. Roe, M. Blaauw, G. T.
518 Swindles, and H. Falck, 2015: Sediment accumulation rates in subarctic lakes: Insights into
519 age-depth modeling from 22 dated lake records from the Northwest Territories, Canada.
520 *Quat. Geochronol.*, **27**, 131-144, http://dx.doi.org/10.1016/j.quageo.2015.02.001.

521 Dibike, Y., T. Prowse, B. Bonsal, L. de Rham, and T. Saloranta, 2012: Simulation of North
522 American lake-ice cover characteristics under contemporary and future climate conditions.
523 *Int. J. Climatol.*, **32**, 695-709, https://doi.org/10.1002/joc.2300.

524 Environment and Climate Change Canada, 2020: Ice Thickness data. Accessed 18 April 2020,
525 https://www.canada.ca/en/environment-climate-change/services/ice-forecasts-
526 observations/latest-conditions/archive-overview/thickness-data.html.

527 FLake, 2020: Useful Hints. Accessed 24 December 2020, https://flake.igb-
528 berlin.de/site/download.

529 Furgal, C., and T. Prowse, 2008: Northern Canada, In: Lemmen, D. S., F. J. Warren, J. Lacroix,
530 E. Bush (Eds.) From impacts to adaptation: Canada in a changing climate 2007.
531 Government of Canada, Ottawa, pp. 57-118.

532 Fyfe, J. C., and Coauthors, 2013: One hundred years of Arctic surface temperature variation
533 due to anthropogenic influence. *Sci. Rep.*, **3**, 2645, http://doi.org/10.1038/srep02645.

534 Galloway, J. M., A. Macumber, R. T. Patterson, H. Falck, T. Hadlari, and E. Madsen, 2010:
535 Paleoclimatological Assessment of the Southern Northwest Territories and Implications for
536 the Long-Term Viability of the Tibbitt to Contwoyto Winter Road, Part I: Core Collection.
537 Northwest Territories Geoscience Office, NWT Open Report 2010-002, 21 pp.

538 Gosling, S., G. McGregor, and J. Lowe, 2009: Climate change and heat-related mortality in six
539 cities part 2: climate model evaluation and projected impacts from changes in the mean and

Accepted for publication in *Bulletin of the American Meteorological Society*. DOI 10.1175/BAMS-D-20-0168.1.

variability of temperature with climate change. *Int. J. Biometeorol*. **53**, 31–51, https://doi.org/10.1007/s00484-008-0189-9.

Hawkins, E., T. M. Osborne, C. Kit Ho, and A. J. Challinor, 2013: Calibration and bias correction of climate projections for crop modelling: An idealised case study over Europe. *Agr. Forest Meteorol.*, **170**, 19-31, http://dx.doi.org/10.1016/j.agrformet.2012.04.007.

Hjort, J., and Coauthors, 2018: Degrading permafrost puts Arctic infrastructure at risk by mid-century. *Nat. Commun.*, **9 (1)**, 5147, https://doi.org/10.1038/s41467-018-07557-4.

Ho, C. K., D. B. Stephenson, M. Collins, C. A. T. Ferro, and S. J. Brown, 2012: Calibration strategies: a source of additional uncertainty in climate change projections. *Bull. Am. Meteorol. Soc*., **93**, 21-26, https://doi.org/10.1175/2011BAMS3110.1.

Hori, Y., V. Y. S. Cheng, W. A. Gough, J. Y. Jien, and L. J. S. Tsuji, 2018: Implications of projected climate change on winter road systems in Ontario's Far North, Canada. *Clim. Change*, **148**, 109-122, https://doi.org/10.1007/s10584-018-2178-2).

Hori, Y., W. A. Gough, K. Butler, and L. J. S. Tsuji, 2016: Trends in the seasonal length and opening dates of a winter road in the western James Bay region, Ontario, Canada. *Theor. Appl. Climatol.*, **129**, 1309-1320, https://doi.org/10.1007/s00704-016-1855-1.

Horton, R., and Coauthors, 2015: Contribution of changes in atmospheric circulation patterns to extreme temperature trends. *Nature*, **522**, 465-469, https://doi.org/10.1038/nature14550.

Huang, A., and Coauthors, 2019: Evaluating and improving the performance of three 1-D lake models in a large deep lake of the Central Tibetan Plateau. *JGR Atmospheres*, **124**, 3143-3167, https://doi.org/10.1029/2018JD029610.

IPCC, 2013: Summary for Policymakers. In: Climate Change 2013: The Physical Science Basis. Contribution of Working Group I to the Fifth Assessment Report of the

Accepted for publication in *Bulletin of the American Meteorological Society*. DOI 10.1175/BAMS-D-20-0168.1.

563 Intergovernmental Panel on Climate Change [Stocker, T.F., and Coauthors (eds.)].
564 Cambridge University Press, Cambridge, United Kingdom and New York, NY, USA.

565 IPCC, 2018: Summary for Policymakers. In: Global Warming of 1.5°C. An IPCC Special
566 Report on the impacts of global warming of 1.5°C above pre-industrial levels and related
567 global greenhouse gas emission pathways, in the context of strengthening the global
568 response to the threat of climate change, sustainable development, and efforts to eradicate
569 poverty [Masson Delmotte, V., and Coauthors (eds.)]. In Press.

570 IPCC, 2019: Summary for Policymakers. In: IPCC Special Report on the Ocean and
571 Cryosphere in a Changing Climate [Pörtner, H.-O., and Coauthors (eds.)]. In Press.

572 Jeffries, M. O., and K. Morris, 2006. Instantaneous daytime conductive heat flow through snow
573 on lake ice in Alaska. *Hydrologic. Process.*, **20**, 803-815,
574 https://doi.org/10.3402/tellusa.v64i0.17614.

575 Jensen, O. P., B. J. Benson, J. J. Magnuson, V. M. Card, M. N. Futter, P. A. Soranno, and K.
576 M. Stewart, 2007: Spatial analysis of ice phenology trends across the Laurentian Great
577 Lakes region during a recent warming period. *Limnol. Oceanogr.*, **52 (5)**, 2013-2026,
578 https://doi.org/10.4319/lo.2007.52.5.2013.

579 JVMC (Joint Venture Management Committee), 2014: Tibbitt to Contwoyto Winter Road Joint
580 Venture. Accessed 6 Feb 2014, www.jvtcwinterroad.ca/jvwr.

581 JVMC (Joint Venture Management Committee), 2015: Tibbitt to Contwoyto Winter Road Joint
582 Venture. Accessed 24 Jan 2015, dev.jvtcwinterroad.ca.

583 JVTC (Joint Venture Trucking Company), 2020: Tibbitt to Contwoyto Winter Road Joint
584 Venture. Accessed 23 April 2020, https://jvtcwinterroad.ca/.

585 Kheyrollah Pour, H., C. R. Duguay, A. Martynov, and L. C. Brown, 2012: Simulation of
586 surface temperature and ice cover of large northern lakes with 1-D models: a comparison

Accepted for publication in *Bulletin of the American Meteorological Society.* DOI 10.1175/BAMS-D-20-0168.1.

587 with MODIS satellite data and in situ measurements. *TELLUS A: Dynamic Meteorology*
588 *and Climatology*, **64:1**, 17614, https://doi.org/10.3402/tellusa.v64i0.17614.

589 Kirillin, G., J. Hochschild, D. Mironov, A. Terzhevik, S. Golosov, and G. Nützmann, 2011:
590 FLake-Global: Online lake model with worldwide coverage. *Environ. Modell. Softw.*, **26**,
591 683-684, https://doi.org/10.1016/j.envsoft.2010.12.004.

592 Kourzeneva, E., 2014: Assimilation of lake water surface temperature observations with
593 extended kalman filter. *Tellus A: Dynamic Meteorology and Oceanography*, **66**, 21510,
594 https://doi.org/10.3402/tellusa.v66.21510.

595 Kwok, R., and Coauthors, 2009: Thinning and volume loss of the Arctic Ocean sea ice cover:
596 2003-2008. *J. Geophys. Res.*, **114**, https://doi.org/10.1029/2009JC005312.

597 Lee, S., T. T. Gong, N. C. Johnson, S. B. Feldstein, and D. Pollard, 2011: On the possible link
598 between tropical convection and the Northern Hemisphere Arctic surface air temperature
599 change between 1958-2001. *J. Clim.*, **24**, 4350-4367,
600 https://doi.org/10.1175/2011JCLI4003.1.

601 Leppäranta, M., 2010: Modelling the formation and decay of lake ice. *The impact of climate*
602 *change on European lakes*, G. George, Ed., Springer, 63-83, https://doi.org/10.1007/978-
603 90-481-2945-4.

604 Melvin, A. M., and Coauthors, 2017: Climate change damages to Alaska public infrastructure
605 and the economics of proactive adaptation. *Proc. Nat. Acad. Sci.*, **114 (2)**, E122-E131,
606 https://doi.org/10.1073/pnas.1611056113.

607 Meredith, M., and Coauthors, 2019: Polar Regions. In: IPCC Special Report on the Ocean and
608 Cryosphere in a Changing Climate Pörtner, H.-O., and Coauthors (eds.)]. In Press.

Accepted for publication in *Bulletin of the American Meteorological Society*. DOI 10.1175/BAMS-D-20-0168.1.

609 Mironov, D. V., 2008: Parameterization of lakes in numerical weather prediction. Description
610 of a lake model. COSMO Technical Report, No. 11, Deutscher Wetterdienst, Offenbach
611 am Main, Germany, 41 pp.

612 Mullan, D., and Coauthors, 2017: Climate change and the long-term viability of the world's
613 busiest heavy haul ice road. *Theor. Appl. Climatol.*, **129**, 1089-1108,
614 https://doi.org/10.1007/s00704-016-1830-x.

615 Najafi, M. R., F. W. Zwiers, and N. P. Gillett, 2015: Attribution of Arctic temperature change
616 to greenhouse-gas and aerosol influences. *Nat. Clim. Change*, **5 (3)**, 246–249,
617 http://doi.org/10.1038/nclimate2524.

618 Nõges, P., and Nõges, T., 2014: Weak trends in ice phenology of Estonian large lakes despite
619 significant warming trends. *Hydrobiologia*, **731**, 5-18.

620 Overland, J. E., and Coauthors, 2015. The melting Arctic and mid-latitude weather patterns:
621 are they connected? *J. Clim.*, **28**, 7917-7932, https://doi.org/10.1175/JCLI-D-14-00822.1.

622 Overland, J., and Coauthors, 2018: The urgency of Arctic change. *Polar Sci.*,
623 https://doi.org/10.1016/j.polar.2018.11.008.

624 Perrin, A., and Coauthors, 2015: Economic implications of climate change adaptations for mine
625 access roads in Northern Canada. Northern Climate ExChange, Yukon Research Centre,
626 Yukon College, 93pp.

627 Pietikäinen, J.-P., and Coauthors, 2018: The regional climate model REMO (v2015) coupled
628 with the 1-D freshwater lake model FLake (v1): Fenno-Scandinavian climate and lakes.
629 *Geosci. Model Dev.*, **11**, 1321-1342, https://doi.org/10.5194/gmd-11-1321-2018.

630 Prowse, T. D., B. R. Bonsal, C. R. Duguay, and M. P. Lacroix, 2007: River-ice break-up/freeze-
631 up: a review of climatic drivers, historical trends and future predictions. *Ann. Glaciol.*, **46**,
632 443-451, https://doi.org/10.3189/172756407782871431.

Accepted for publication in *Bulletin of the American Meteorological Society*. DOI 10.1175/BAMS-D-20-0168.1.

633 Rodan, G., 2012: Storm strands truckers. Northern News Services, March 19, 2012. Accessed
634 30 May 2020, www.nnsl.com/preview/newspapers/stories/mar21_12rd.html.

635 Rontu, L., K. Eerola, and M. Horttanainen, 2019: Validation of lake surface state in the
636 HIRLAM v.7.4 numerical weather prediction model against in situ measurements in
637 Finland. *Geosci. Model Dev.*, **12**, 3707-3723, https://doi.org/10.5194/gmd-12-3707-2019.

638 Shabbar, A., M. Khandekar, 1996: The impact of El Niño-Southern Oscillation on the
639 temperature field over Canada. *Atmos. Ocean*, **34**, 401-416,
640 https://doi.org/10.1080/07055900.1996.9649570.

641 Sim, T. G., G. T. Swindles, P. J. Morris, M. Gałka, D. Mullan, and J. M. Galloway, 2019:
642 Pathways for ecological change in Canadian High Arctic wetlands under rapid twentieth
643 century warming. *Geophys. Res. Lett.*, **46**, 4726–4737,
644 https://doi.org/10.1029/2019GL082611.

645 Sladen, W. E., S. A. Wolfe, and P. D. Morse, 2020: Evaluation of threshold freezing conditions
646 for winter road construction over discontinuous permafrost peatlands, subarctic Canada.
647 *Cold Reg. Sci. Technol.*, **170**, 102930, https://doi.org/10.1016/j.coldregions.2019.102930.

648 Swindles, G. T., and Coauthors, 2015: The long-term fate of permafrost peatlands under rapid
649 climate warming. *Sci. Rep.*, **5**, 17951, https://doi.org/10.1038/srep17951.

650 Taylor, K. E., R. J. Stouffer, and G. A. Meehl, 2012: An overview of CMIP5 and the
651 experiment design. *Bull. Amer. Meteor. Soc.*, **93**, 485-498. https://doi.org/10.1175/BAMS-
652 D-11-00094.1.

653 Timmermann, A., and Coauthors, 2018: El Niño–Southern Oscillation complexity. *Nature*,
654 **559**, 535-545, https://doi.org/10.1038/s41586-018-0252-6.

Accepted for publication in *Bulletin of the American Meteorological Society*. DOI 10.1175/BAMS-D-20-0168.1.

655 UNFCCC, 2015: Paris Agreement. Accessed 26 June 2020,
656 https://unfccc.int/files/essential_background/convention/application/pdf/english_paris_ag
657 reement.pdf.

658 van Vuuren, D. P., and Coauthors, 2011: The representative concentration pathways: an
659 overview. *Clim. Change*, **109**, 5-31, https://doi.org/10.1007/s10584-011-0148-z.

660 Wallace, J. M., and D. S. Gutzler, 1981: Teleconnections in the Geopotential Height Field
661 during the Northern Hemisphere Winter. *Mon. Wea. Rev.*, **109 (4)**, 784-812,
662 https://doi.org/10.1175/1520-0493(1981)109<0784:TITGHF>2.0.CO;2.

663 Weedon, G. P., G. Balsamo, N. Bellouin, S. Gomes, M. J. Best, and P. Viterbo, 2014: The
664 WFDEI meteorological forcing data set: WATCH Forcing Data methodology applied to
665 ERA- Interim reanalysis data. *Water Resour. Res.*, **50**, 7505-7514,
666 https://doi.org/10.1002/2014WR015638.

667 Yang, W., and G. Magnusdottir, 2018: Year-to-year variability in Arctic minimum sea ice
668 extent and its preconditions in observations and the CESM large ensemble simulations. *Sci.*
669 *Rep.*, https://doi.org/10.1038/s41598-018-27149-y.

670 Yang, Y., B. Cheng, E. Kourzeneva, T. Semmler, L. Rontu, M. Leppäranta, K. Shirasawa, and
671 Z. J. Li, 2013: Modelling experiments on air-snow-ice interactions over Kilpisjärvi, a lake
672 in northern Finland. *Boreal Environ. Res.*, **18**, 341-358.

673
674
675
676
677
678

Accepted for publication in *Bulletin of the American Meteorological Society*. DOI 10.1175/BAMS-D-20-0168.1.

679 **Appendix Tables**

680

Model Ensemble	RMSE	1.5°C	2°C	4°C
IPSL-CM5A-LR r1i1p1	1.16	2033-2053	2039-2059	2074-2094
ICHEC EC-Earth r2i1p1	1.42	2029-2049	2047-2067	
NOAA GFDL-ESM2G r1i1p1	1.52	2037-2057	2058-2078	
CSIRO-QCCCE CSIRO-Mk3-6-0 r9i1p1	1.54	2031-2051	2043-2063	
IPSL-CM5A-LR r4i1p1	1.37	2027-2047		
CSIRO-QCCCE CSIRO-Mk3-6-0 r8i1p1	1.46		2048-2068	
IPSL-CM5A-LR r3i1p1	1.78			2075-2095
MIROC5 r2i1p1	1.82			2066-2086
MIROC5 r3i1p1	1.90			2069-2089
CSIRO-QCCCE CSIRO-Mk-3-6-0 r1i1p1	1.92			2079-2099

681

682 **Table A1.** All 15 shortlisted scenarios as used for FLake modelling. Root Mean Square Error
683 (RMSE) is provided, along with the extracted years for each scenario. Twenty-year time
684 periods were taken from 1 October on the start year to 30 September on the end year to conform
685 to the temporal basis of FLake modelling and represent the 20-year mean period when
686 temperatures first exceed the RMTI associated with each of the three GMTIs.

687

688

689

690

691

692

Accepted for publication in *Bulletin of the American Meteorological Society.* DOI 10.1175/BAMS-D-20-0168.1.

Year	Open Date	Close Date	Duration (Days)	No. Loads	Tonnes
2001	1 Feb	13 Apr	72	7,981	245,586
2002	26 Jan	16 Apr	81	7,735	256,915
2003	1 Feb	2 Apr	61	5,243	198,818
2004	28 Jan	31 Mar	63	5,091	179,144
2005	26 Jan	5 Apr	70	7,607	252,533
2006	4 Feb	26 Mar	50	6,841	177,674
2007	27 Jan	9 Apr	73	10,922	330,002
2008	29 Jan	7 Apr	62	7,484	245,585
2009	1 Feb	25 Mar	50	5,377	173,195
2010	4 Feb	24 Mar	46	3,508	120,020
2011	28 Jan	31 Mar	63	6,832	239,000
2012	1 Feb	28 Mar	59	6,551	210,188
2013	30 Jan	31 Mar	61	6,017	223,206
2014	30 Jan	1 Apr	62	7,069	243,928
2015	30 Jan	31 Mar	61	8,915	305,215
2016	9 Feb	24 Mar	44	8,766	262,261
2017	1 Feb	29 Mar	57	8,241	279,484
2018	1 Feb	31 Mar	61	8,209	303,725
2019	1 Feb	31 Mar	59	7,489	257,176
2020	31 Jan	8 Apr	68	7,072	230,497

693

694 **Table A2.** Historical Operational Season Statistics for the TCWR (JVTC, 2020).

695

696

Accepted for publication in *Bulletin of the American Meteorological Society.* DOI 10.1175/BAMS-D-20-0168.1.

Figures

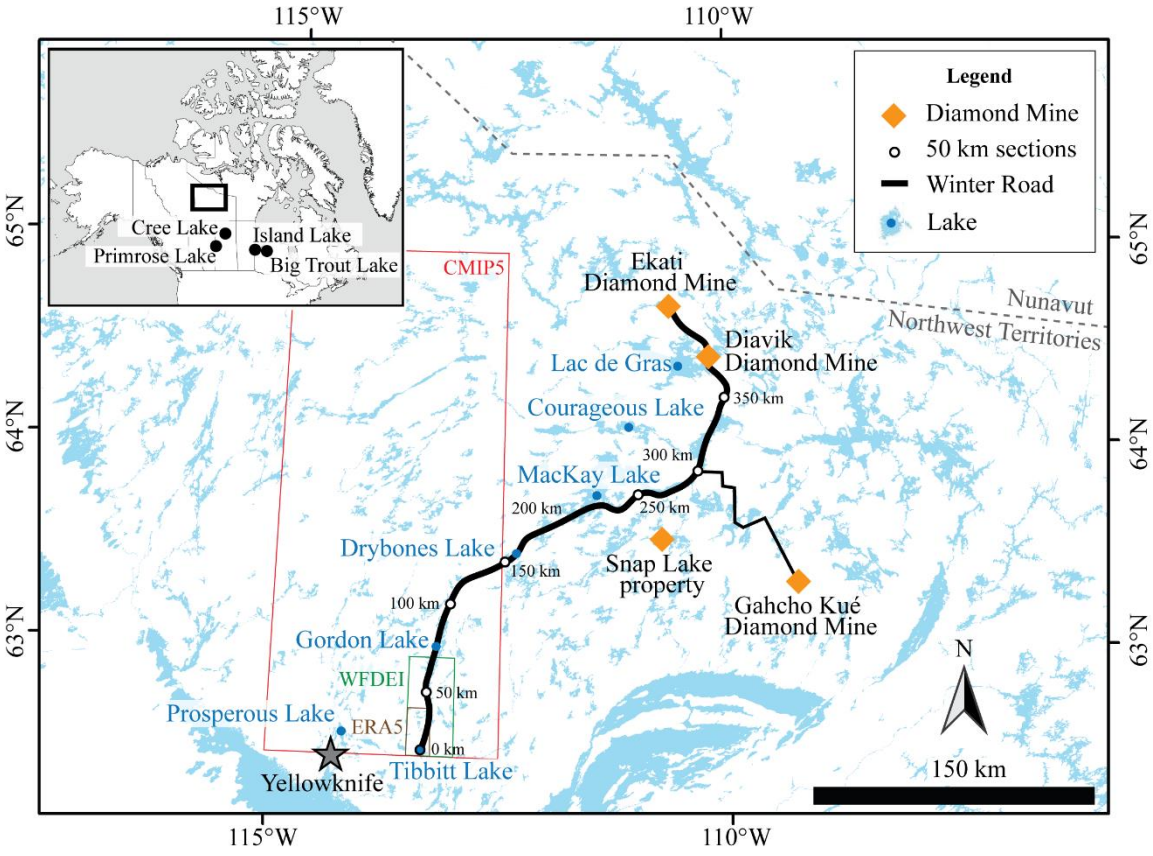

Figure 1. The TCWR study region. The three transparent boxes show the spatial resolution of the ERA5 (0.25° x 0.25°) and WFDEI (0.5° x 0.5°) climate observations, as well as the CMIP5 climate model scenarios (*ca.* 2.5° x 2.5° but variable from model to model). The locations of the four lakes used for model validation are also shown in the inset map.

Accepted for publication in *Bulletin of the American Meteorological Society.* DOI 10.1175/BAMS-D-20-0168.1.

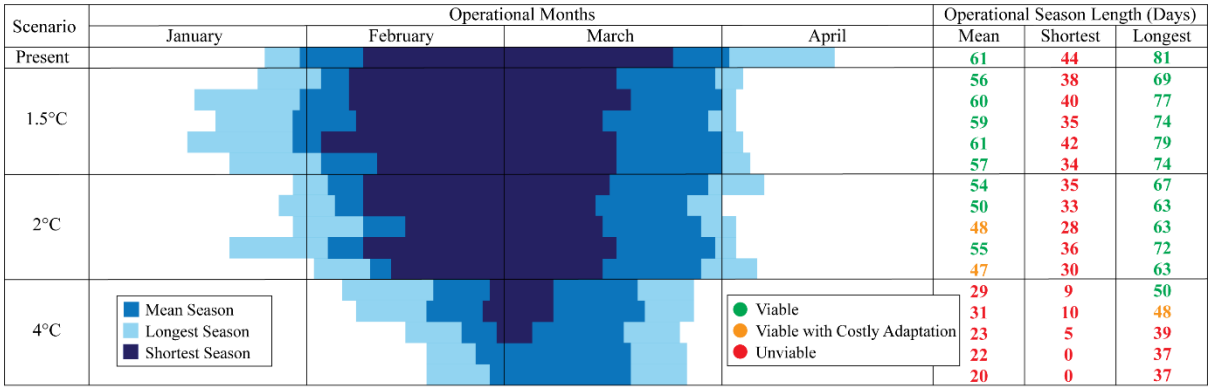

Figure 2. TCWR operational season as observed for the present (mean of 2001-2020 observations taken from JVTC (2020)) (n=1) and simulated by FLake for the future under 15 climate scenarios corresponding to a GMTI of 1.5°C (n=5), 2°C (n=5) and 4°C (n=5). The mean of the 20-year observations / simulations is shown in medium blue, while the year with the shortest (longest) season is shown in dark (light) blue. Also shown is the operational season length (days) for the mean, shortest and longest years in a traffic light colour system following the scenarios outlined in Perrin et al. (2015): ≥ 50 days = green (viable); 45-49 days = amber (viable with costly adaptation); < 45 days = red (unviable).

Accepted for publication in *Bulletin of the American Meteorological Society.* DOI 10.1175/BAMS-D-20-0168.1.

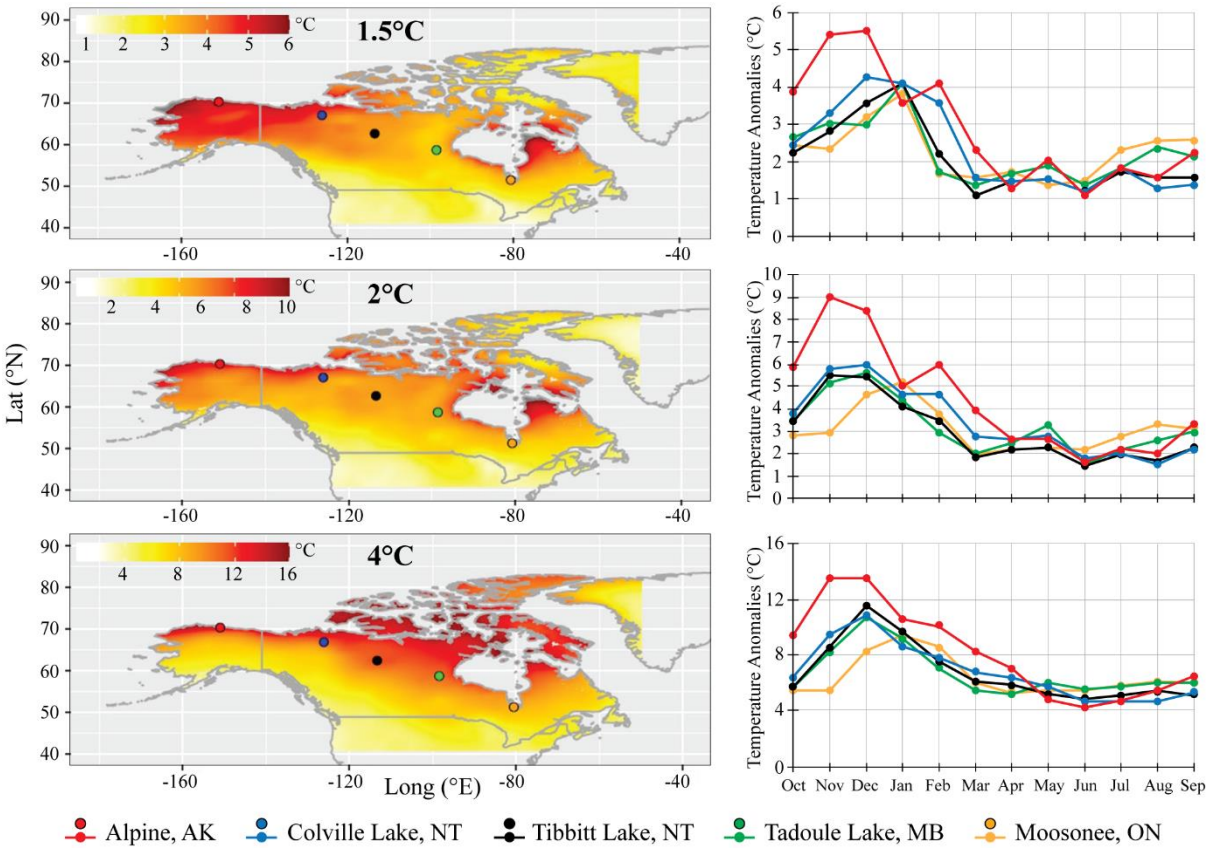

717

718 **Figure 3.** Map panels: mean projected December temperature anomalies for the northern half
719 of North America. Temperature anomalies are expressed as the mean of the models analysed
720 in this study at a GMTI of 1.5°C, 2°C and 4°C from the mean 1986-2005 observed period.
721 Graph panels: Temperature anomalies (calculated in the same way as above) for each month
722 of the year for five winter roads in North America (including the TCWR, as represented by
723 Tibbitt Lake, NT). Two-letter state/province/territory codes are used for the five winter road
724 locations – AK: Alaska; MB: Manitoba; NT: Northwest Territories; ON: Ontario.

725

Accepted for publication in *Bulletin of the American Meteorological Society.* DOI 10.1175/BAMS-D-20-0168.1.

726 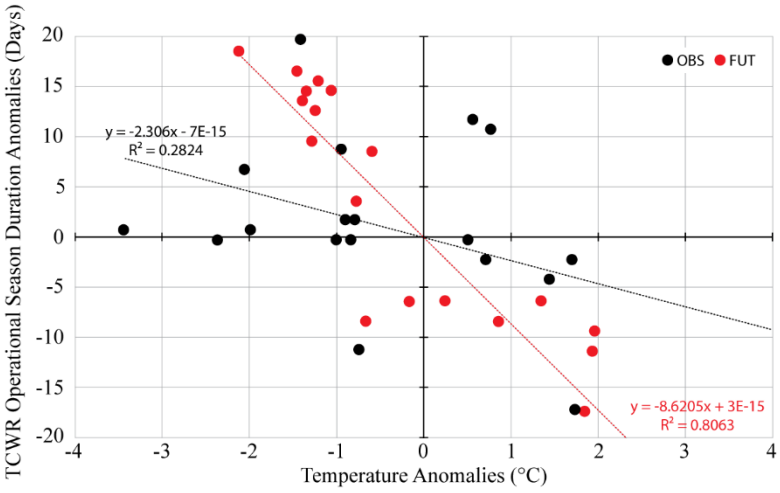

727 **Figure 4. November-April mean** temperature (°C) and TCWR seasonal duration (days)
728 anomalies for the Tibbit Lake region of the TCWR. Anomalies for each year of the 20-year
729 observed record / model simulations are expressed as changes relative to the mean of that same
730 20-year period. Black points represent observations (OBS) for 2000-2020 and red points
731 represent the most extreme model simulation (FUT) under a 4°C GMTI – in this case for 2079-
732 2099 – the 20-year period when temperatures first rise the RMTI equivalent of 4°C GMTI
733 above preindustrial temperatures.

734

Accepted for publication in *Bulletin of the American Meteorological Society.* DOI 10.1175/BAMS-D-20-0168.1.

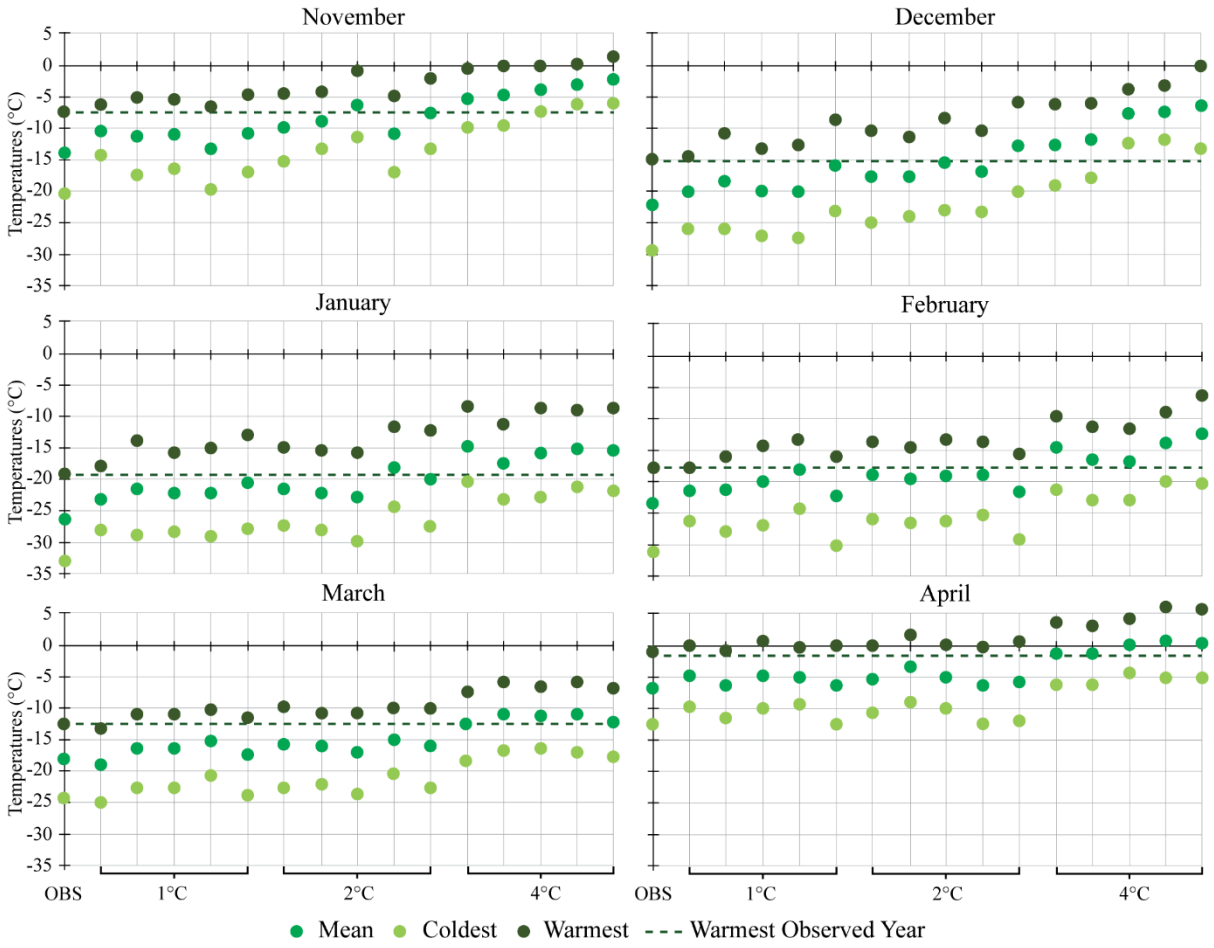

Figure 5. November-April temperatures at Tibbitt Lake as observed (OBS) for the present (n=1) and simulated for the future under 15 climate scenarios corresponding to a GMTI of 1.5°C (n=5), 2°C (n=5) and 4°C (n=5). The mean of the 20-year observations / simulations is shown in medium green, while the year with the coldest (warmest) temperatures for each particular month is shown in light (dark) green. The dashed line represents observed temperatures during the warmest year (mean of November-April).

Accepted for publication in *Bulletin of the American Meteorological Society.* DOI 10.1175/BAMS-D-20-0168.1.

Appendix Figures

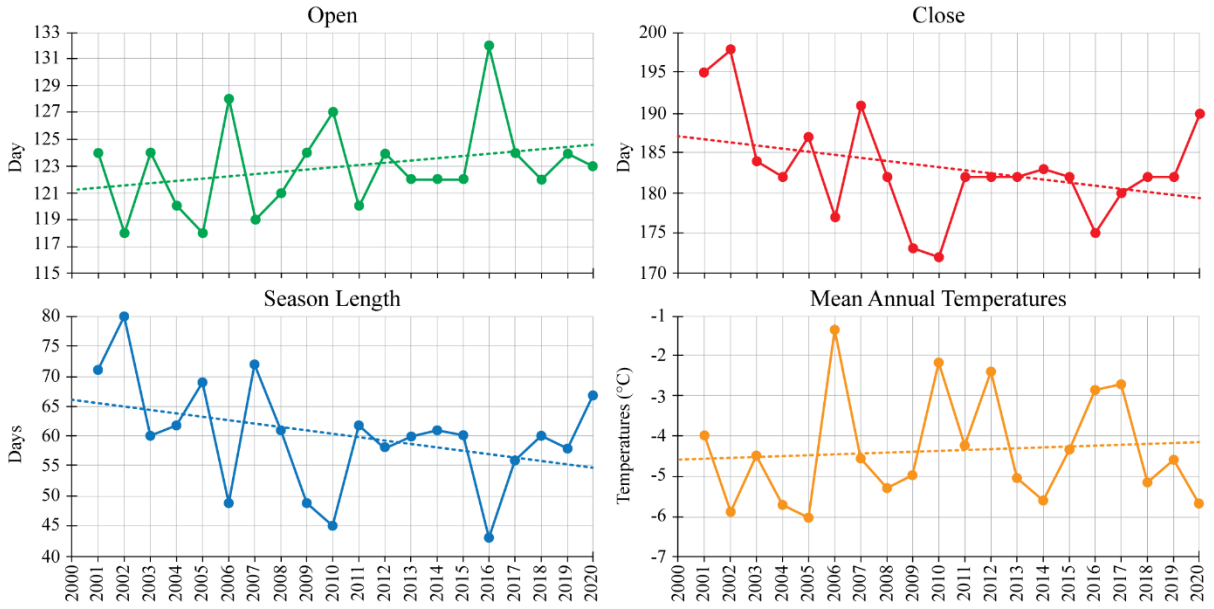

Figure A1. Changes in the TCWR open date (top left) and close date (top right) from 2001-2020 (JVTC, 2020) and mean annual air temperatures for Tibbitt Lake from 2001-2020. For the top panels and the bottom left panel, dates are expressed as days since the start of the hydrological year on 1 October. Mean annual air temperatures are calculated for hydrological years, starting on 1 October and ending on 30 September the next year.

Accepted for publication in *Bulletin of the American Meteorological Society.* DOI 10.1175/BAMS-D-20-0168.1.

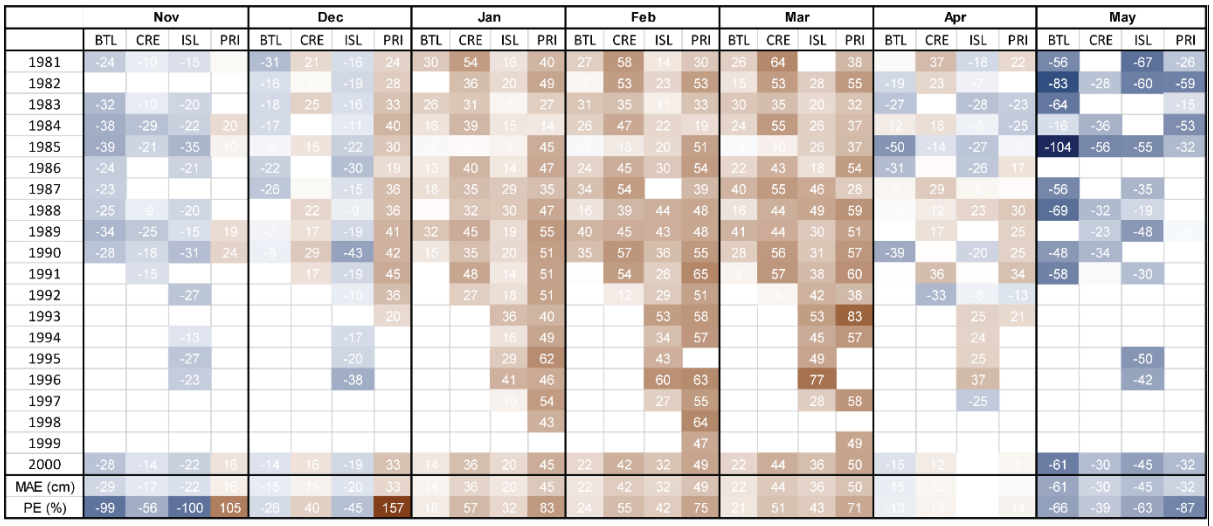

Code	Name	Province	Latitude (°)	Longitude (°)	Fetch (km)	Mean Depth (m)	FU Bias (Days)	BU Bias (Days)
BTL	Big Trout Lake	Ontario	53.76	-90.08	4.3	16.0	-14	13
CRE	Cree Lake	Saskatchewan	57.41	-106.41	3.0	14.9	2	14
ISL	Island Lake	Manitoba	53.87	-94.65	2.5	20.1	-17	7
PRI	Primrose Lake	Saskatchewan / Alberta	54.91	-109.68	3.6	9.8	16	2
						Mean	-3	9

Figure A2. Absolute error (observed ice thickness minus modelled ice thickness) for four analogous shallow sub-arctic Canadian lakes (the details of which are provided in the table part of the figure) covering a minimum of ten years during the period 1981-2000. Results are provided on a monthly basis, with mean absolute error (MAE) calculated for all years with measurements and percentage error (PE) calculated as relative error multiplied by 100. Also provided in the table part of the figure is freezeup (FU) bias and breakup (BU) bias – calculated as observed FU/BU minus FLake simulated FU/BU for each lake across the same years as the data used to calculate absolute error in the main part of the figure. Negative (positive) numbers indicate FU/BU is simulated later (earlier) than observed.

Accepted for publication in *Bulletin of the American Meteorological Society.* DOI 10.1175/BAMS-D-20-0168.1.